AIAA 2015-0772

SciTech2015
5-9 January, 2015, Kissimmee, FL
53rd AIAA Aerospace Sciences Meeting

Design of High Wing Loading Compact Electric Airplane Utilizing Co-Flow Jet Flow Control

Alexis Lefebvre [*], G.-C. Zha [†]
Dept. of Mechanical and Aerospace Engineering
University of Miami
Coral Gables, Florida 33124
E-mail: gzha@miami.edu

Abstract

This paper presents a conceptual electric airplane design utilizing Co-Flow Jet (CFJ) flow control. The purpose is to design an aircraft with high wing loading and a compact size so that an airplane can carry more battery and reach a longer range. The CFJ Electric Aircraft (CFJ-EA) mission is to carry 4 passengers at a cruise Mach number of 0.15 with a range of about 300nm. The CFJ-EA cruises at a very high C_L of 1.3, which produces a wing loading of $182.3 kg/m^2$, about 3 times higher than that of a conventional general aviation airplane. The aerodynamic efficiency including the power consumption of the CFJ pump $(L/D)c$ is excellent with a value of 24 at a low momentum coefficient C_μ of 0.04. Takeoff and landing distances are also reasonable due to a very high maximum C_L of 4.8, achieved with a high C_μ of 0.28. The wing is designed to pivot around its 1/4 chord axis so that it can achieve high angle of attack (AoA) without rotating the fuselage. A measure of merit defined as PMS=Passengers*Miles/S is introduced, where S is the wing planform area. The PMS of the present EA design is close to that of a conventional reciprocating engine general aviation airplane, and is 2.3 to 3.8 times greater than the PMS of the state of the art EA. The design results suggest that the CFJ-EA has a far greater range than a same size EA using a conventional wing design. Or for the same range, the CFJ-EA has a much smaller size than a conventional design. This design is the first trail with no systematic design optimization. The CFJ-EA concept may open the door to a new class of general aviation EA designs. The same CFJ flow control technology can also be used for other general aviation airplanes with conventional propulsion systems and for high altitude airplanes to reduce size.

[*] Graduate Student
[†] Professor, AIAA Associate Fellow

Nomenclature

AoA	Angle of attack
CFJ	Co-flow jet
SSM	Static stability margin
TOL	Takeoff and landing
EA	Electric aircraft
LE	Leading edge
TE	Trailing edge
GA	General aviation
S	Planform area
V	Flow velocity
ρ	Air density
$\dot{m}$	Mass flow
M	Mach number
L	Aircraft lift
D	Aircraft Drag
p	Static pressure
P	Pumping power
C_L	Lift coefficient $L/(q_\infty S)$
C_D	Drag coefficient $D/(q_\infty S)$
C_M	Moment coefficient $\omega/(q_\infty S\, c)$
C_p	Pressure coefficient $(p - p_\infty)/q_\infty$
C_μ	Jet momentum coefficient. $\dot{m}_j\, U_j/(q_\infty S)$
Pc	Power coefficient $L/(q_\infty S\, V_\infty)$
E^*	Battery specific energy density (Wh/kg)
R	Aircraft range
t	Cruise time
W_b	Battery mass(kg)
P_b	Battery power drawn (W)
(L/D)	Aerodynamic efficiency
$(L/D)c$	CFJ corrected efficiency $L/(D\, P/V_\infty)$
∞	Free stream conditions
$_j$	Jet conditions

1 Introduction

The main challenge of general aviation (GA) electric airplanes (EA) resides in the limited amount of energy that can be carried on board of the aircraft. The specific energy density of Li-ion battery is typically 60 times lower than that of kerosene. Hence for the same weight, the energy stored on an electric plane will only be a fraction of its kerosene counterpart. This drastically limits the GA EA range and payload. Due to this limitation, today's GA EA are usually 1 or 2 passenger aircraft with a range typically shorter than 100nm. To mitigate the range limitation, a GA EA often adopts a glider design with high aspect ratio and low wing loading to achieve maximum aerodynamic efficiency.

The e-Genius shown in Fig. 1 is a typical configuration example of the current GA EA, which has a large aspect ratio of 19.6 and a payload of 2 passengers. The design is very successful and set 7 world record as of July 2014. The Taurus G4 shown in 2, won the 2011 Green Flight Challenge. By combining

two fuselages, the Taurus G4 achieves an aspect ratio of 22.5 and is the first 4 passengers EA. Both the e-genius and the Taurus G4 have a range over 200nm due to a very high cruise L/D ratio of about 28. However, both designs have a relatively low cruise wing loading, which limits the amount of battery they can carry and their range. To increase the range of EAs without increasing their size, the cruise wing loading must be increased. A conventional aircraft can not achieve a high cruise wing loading while keeping a reasonable cruise aerodynamic efficiency. In addition, a high cruise wing loading leads to a smaller stall margin and longer takeoff and landing (TOL) distances. To overcome the limitation of low cruise wing loading, a revolutionary new concept aircraft design must be pursued.

Figure 1: The e-Genius broke 7 world records in July 2014.

Figure 2: The Taurus G4 airplane, winner of the Green Flight Challenge in 2011, Image by Wernher Krutein / Photovault.com

The advanced co-flow jet (CFJ) flow control airfoil recently developed by Zha and his team [1, 2, 3, 4, 5, 6, 7, 8, 9] offers a promising new concept that can significantly increase the cruise wing loading with a high aerodynamic efficiency, low energy expenditure and high stall AoA. In the CFJ airfoil concept,

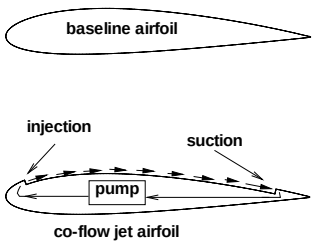

Figure 3: CFJ airfoil concept

an injection slot near the leading edge (LE) and a suction slot near the trailing edge (TE) on the airfoil suction surface are created as sketched in Fig. 3. A small mass flow is withdrawn into the airfoil near the TE, pressurized and energized by a pumping system inside the airfoil, and then injected near the LE tangentially to the main flow. The whole process does not add any mass flow to the system and hence is a zero-net mass-flux (ZNMF) flow control.

An advantage of the zero-net mass-flux flow control airfoil, is that the drag measured by the wind tunnel balance is the total drag of the airfoil like conventional airfoil. No additional drag will be generated such as the ram drag of circulation control airfoil that uses blowing only on the airfoil [2]. The maximum aerodynamic L/D of CFJ is usually very high since the CFJ significantly reduces the drag or even generate thrust. The aerodynamic lift and drag will be used for the aircraft design to size the payload and engine thrust required. For an active flow control airfoil however, the measure of aerodynamic efficiency can not use the conventional definition of L/D, but needs to consider the energy consumption for the flow control. The proper aerodynamic efficiency for CFJ airfoil is hence defined as :

$$(\frac{L}{D})_c = \frac{L}{D + P/V_\infty} \tag{1}$$

where P is the power consumed by the active flow control system, V_∞ is the freestream speed.

At the maximum $(L/D)_c$, a CFJ airfoil usually has a higher C_L than that of a conventional airfoil. Hence the CFJ wing is able to cruise at a much higher wing loading. As a result, the battery payload and the range would be greatly increased by using a CFJ airplane. In addition, a CFJ wing can achieve a very high maximum C_L of about 5.0, which removes the takeoff distance penalty usually occurring for high wing loading aircraft.

The CFJ wing is used for the whole flight mission without additional high lift flap or slat systems. At takeoff and landing phase when the high maximum lift coefficient is needed, the maximum CFJ pumping power is utilized. At cruise, a small pumping power is used to achieve high cruise lift and high aerodynamic efficiency. The wing weight could be reduced due to the absence of moving parts.

The motivation for developing electric aviation is driven by the necessity for mankind to lower the carbon emission footprint. While the EA performance is not expected to reach those of internal combustion airplanes in the short term, continuous improvements in electric storage coupled with the price increased of kerosene could make the GA EA market grow considerably in the near future. More information about electricity storage technologies and electric planes can be found in [10]. Short distance flights are particularly suitable for EA because they require less energy overall and hence the battery weight is less of an issue.

In the past, two attempts were made to use CFJ airfoils for integrated propulsion-lifting system of flying wings. The two airplanes, "Engineless" CFJ Aircraft (ECA) [11] and QUEIA [12], emphasize on the lift increase and drag decrease provided by the use of CFJ on flying wings. This paper conducts a CFJ electric aircraft (CFJ-EA) design with numerically computed aerodynamic performance, stability margins and power consumption. The present CFJ Electric Aircraft (CFJ-EA) mission is to carry 4 passengers at cruise Mach number of 0.15 with the range about 300nm.

2 CFJ Parameters

This section will introduce the definitions of several parameters that are used to describe a CFJ airfoil performance.

2.1 Lift and Drag Calculation

The momentum and pressure at the injection and suction slots produce a reactionary force, which is automatically measured by the force balance in wind tunnel testing. However, for CFD simulation, the full reactionary force needs to be included. Using control volume analysis, the reactionary force can be calculated using the flow parameters at the injection and suction slot opening surfaces. Zha et al. [2] give the following formulations to calculate the lift and drag due to the jet reactionary force for a CFD simulation. By considering the effects of injection and suction jets on the CFJ airfoil, the expressions for these reactionary forces are given as :

$$F_{x_{cfj}} = (\dot{m}_j V_{j1} + p_{j1} A_{j1}) * cos(\theta_1 - \alpha) - (\dot{m}_j V_{j2} + p_{j2} A_{j2}) * cos(\theta_2 + \alpha) \tag{2}$$

$$F_{y_{cfj}} = (\dot{m}_{j1} V_{j1} + p_{j1} A_{j1}) * sin(\theta_1 - \alpha) + (\dot{m}_{j2} V_{j2} + p_{j2} A_{j2}) * sin(\theta_2 + \alpha) \tag{3}$$

where the subscripts 1 and 2 stand for the injection and suction respectively, and θ_1 and θ_2 are the angles between the injection and suction slot's surface and a line normal to the airfoil chord. α is the angle of attack.

The total lift and drag on the airfoil can then be expressed as:

$$D = R'_x - F_{x_{cfj}} \tag{4}$$

$$L = R'_y - F_{y_{cfj}} \tag{5}$$

where R'_x and R'_y are the surface integral of pressure and shear stress in x (drag) and y (lift) direction excluding the internal ducts of injection and suction. For the CFD simulation, the total lift and drag are calculated using Eqs.(4) and (5).

2.2 Jet Momentum Coefficient

The jet momentum coefficient C_μ is a parameter used to quantify the jet intensity. It is defined as :

$$C_\mu = \frac{\dot{m} V_j}{\frac{1}{2} \rho_\infty {V_\infty}^2 S} \tag{6}$$

where $\dot{m}$ is the injection mass flow, V_j the injection velocity, ρ_∞ and V_∞ denote the free stream density and velocity, and S is the planform area.

2.3 Power Coefficient

The CFJ can be implemented by mounting a pumping system inside the wing that withdraws air from the suction slot and blows it into the injection slot. The power consumption can be determined by the jet mass flow and total enthalpy change as the following :

$$P = \dot{m}(H_{t1} - H_{t2}) \tag{7}$$

where H_{t1} and H_{t2} are the total enthalpy in the injection cavity and suction cavity respectively, P is the Power required by the pump and $\dot{m}$ the jet mass flow rate. Introducing the pump efficiency η and total pressure ratio of the pump $\Gamma = \frac{P_{t1}}{P_{t2}}$, the power consumption can be expressed as :

$$P = \frac{\dot{m} C_p T_{t2}}{\eta}(\Gamma^{\frac{\gamma-1}{\gamma}} - 1) \tag{8}$$

where γ is the specific heat ratio equal to 1.4 for air. The power consumption can be expressed as a power coefficient below:

$$P_c = \frac{P}{\frac{1}{2}\rho_\infty V_\infty^3 S} \tag{9}$$

2.4 Corrected Aerodynamic Efficiency

The conventional airfoil aerodynamic efficiency is defined as :

$$\frac{L}{D} \tag{10}$$

For the CFJ airfoil, the ratio above still represents the pure aerodynamic relationship between lift and drag. However since CFJ active flow control consumes energy, the ratio above is modified to take into account the energy consumption of the pump. The formulation of the corrected aerodynamic efficiency for CFJ airfoils is :

$$(\frac{L}{D})_c = \frac{L}{D + \frac{P}{V_\infty}} \tag{11}$$

where V_∞ is the free stream velocity, P is the pumping power, and L and D are the lift and drag generated by the CFJ airfoil. The formulation above converts the power consumed by the CFJ into a force $\frac{P}{V_\infty}$ which is added to the aerodynamic drag D. If the pumping power is set to 0, this formulation returns to the aerodynamic efficiency of a conventional airfoil.

3 Range Estimate for Electric Aircraft

Unlike conventional reciprocating engine aircraft whose weight is reduced as the fuel is burned, the electric aircraft mass remains constant during the flight and thus the range must be calculated accordingly[10].

Using relations similar to the reciprocating engine aircraft, the energy consumption of the EA is estimated to 2.5% for the start-up and take-off, 7% acceleration to cruise velocity and altitude and 2.5% for the landing phase. In addition, an extra 8% of the battery power should be kept stored in the battery as a safety measure. Thus the specific energy density available for the the cruise out to destination flight phase is

$$E_c = 0.8 \cdot E^* \tag{12}$$

where E^* is the specific energy density of the fully charged battery.

The range of an aircraft is then defined by

$$R = V \cdot t \tag{13}$$

where R is the range, V the cruise velocity and t the cruise time of the aircraft.

The cruise time is equal to the time to drain the battery, which under ideal conditions is

$$t = \frac{W_b \cdot E_c}{P_b} \tag{14}$$

where W_b is the mass of the battery and P_b the power drawn from the battery.

Substituting t to the range equation yields

$$R = \frac{W_b \cdot E_c}{P_b} \cdot V \tag{15}$$

The power drawn from the battery relates to the propulsive power required by the aircraft and the total efficiency of the propulsion system as follow

$$P_b = \frac{P_p}{\eta} \tag{16}$$

Where η is the propeller efficiency and a value of 0.75 is used in this design.

The propulsion power required by the aircraft relates to its weight, lift over drag ratio (L/D) and flight velocity as follow

$$P_p = D \cdot V = \frac{W \cdot g}{L/D} V \tag{17}$$

where W is the weight of the aircraft.

combining Eqs. 16 and 17, the battery power becomes

$$P_b = \frac{W \cdot g}{L/D \cdot \eta} V \tag{18}$$

substituting P_b into Eq. **??** yields

$$\begin{aligned} R &= E_c \cdot \eta \cdot \frac{1}{g} \cdot (\frac{L}{D})_c \cdot \frac{W_b}{W} \\ &= E_c \cdot \eta \cdot \frac{1}{g} \cdot (\frac{L}{D})_c \cdot (1 - \frac{W_p}{W} - \frac{W_s}{W}) \\ &= E_c \cdot \eta \cdot \frac{1}{g} \cdot (\frac{L}{D})_c \cdot (1 - \frac{W_p}{W} - SF) \end{aligned} \tag{19}$$

where SF is the structure factor, which is the ratio of the empty structure weight to the gross weight. In this design, a moderate SF of 0.45 is used. In general, the more compact the airplane size, the smaller the structure factor will be. Eq. (19) indicates that for a constant L/D, payload and structure factor, increasing the gross weight will result in increasing the battery weight, and hence will give the airplane a longer distance. This is the theoretical basis for a high wing loading compact EA to increase range.

4 Aircraft Configuration

The present CFJ-EA geometry with dimensions is shown on the isometric views in Fig. 4. The center of gravity, around which the moments are calculated, is located 2.43 meters from the aircraft nose, slightly bellow the fuselage longitudinal axis as indicated by the pin on the side view.

The present EA wing geometry is based on the result of a trade study conducted in [13]. A simple rectangular wing planform with a thick CFJ airfoil (21% thickness/chord) is chosen as a compromise between wing performance, manufacturing simplicity and structural weight of the wing. The CFJ airfoil, seen in Fig. 5 is based on the NACA 6421 airfoil, with an injection and slot located at 2% chord and 80% chord respectively. The injection and suction size are 0.65% chord and 1.30% chord respectively. The CFJ wing performance and energy consumption is studied in detailed in [13]. It combines very high wing loading with a high aerodynamic efficiency and the energy expenditure is low.

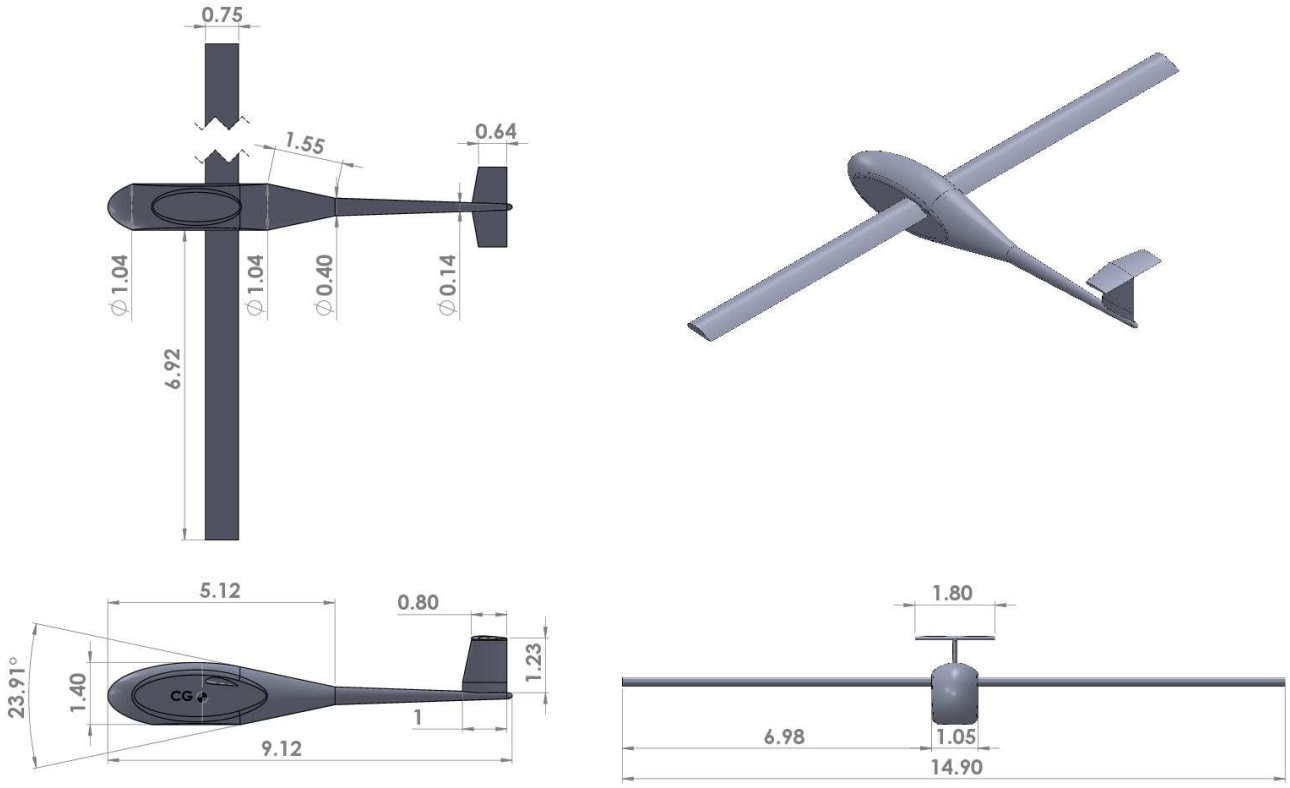

Figure 4: CFJ-EA isometric view (unit: meters).

At cruise, the CFJ-EA fuselage is horizontal and the wing AoA is 5°. At TOL, the wing AoA is 25°. To reach such a high AoA without rotating the fuselage excessively, the wing rotates by 15° around its spar axis. The remaining 5° are achieved by rotation of the fuselage. The moderate fuselage AoA ensures a good visibility for the pilot during the TOL phases. The wing placement on a high position directly behind the passengers is chosen to allow the wing spar to go through the fuselage without affecting the passenger headroom and leaves the space bellow for battery storage. The side surface of the fuselage is flat so that the wing can be rotated around the wing spar axis.

The tail is sized to achieve stability in pitch and sufficient control authority. Both the horizontal

and vertical tail uses a NACA 0012 airfoil. The horizontal and vertical tail sizes are 1.3m^2 and 1.0m^2 respectively. The wing area is 10.44m^2 and the wing span is 14.90m, which gives the CFJ-EA an aspect ratio of 21.3. The fuselage length is 9.12m. The cabin size is constructed from an ellipsoid body with a major axis of 4m, a minor axis of 1.5m and a vertical axis of 1.5m to which we flattened the bottom and the side surfaces. Its final dimensions are 4.0m x 1.4m x 1.05m (Length x Height x Width) and the internal volume is 4.3m^3. Less than 1m^3 is expected to be used for battery and related power equipment. The rest of the volume is used to accommodate the 4 passengers with luggage and the wing rotation system.

5 CFD Simulation Setup

5.1 CFD Code

The FASIP (Flow-Acoustics-Structure Interaction Package) CFD code is used to conduct the numerical simulation. The Reynolds averaged Navier-Stokes (RANS) equations with one-equation Spalart-Allmaras [14] turbulence model is used. A 5th order WENO scheme for the inviscid flux [15, 16, 17, 18, 19, 20] and a 4th order central differencing for the viscous terms [15, 19] are employed to discretize the Navier-Stokes equations. The low diffusion E-CUSP scheme used as the approximate Riemann solver suggested by Zha et al [16] is utilized with the WENO scheme to evaluate the inviscid fluxes. Implicit time marching method using Gauss-Seidel line relaxation is used to achieve a fast convergence rate [21]. Parallel computing is implemented to save wall clock simulation time [22]. The cruise simulation are performed at Mach number 0.15 and the TOL simulations are performance at Mach number 0.10. The Reynolds number, based on the chord of the wing, is 2.6×10^6 and 1.8×10^6 respectively. The RANS solver is validated for CFJ static airfoil simulation [8, 5, 23] and for the DLR-F6 wing/body lift, drag and moment prediction.

5.2 Boundary Conditions

The 3rd order accuracy no slip condition is enforced on the solid surface with the wall treatment suggested in [24] to achieve the flux conservation on the wall. Total pressure, total temperature and flow angles are specified as the inlet boundary conditions for the upstream portion of the farfield boundary and inside the injection cavity. Constant static pressure is used for the downstream portion of the farfield boundary and inside the suction cavity. Symmetry boundary is used in the center of the aircraft in order to reduce the mesh size.

To achieve zero net mass flux with the CFJ flow control, the mass flow exiting the injection slot must be equal to the mass flow entering the suction slot. Additionally, the jet strength must be controlled in order to reach the prescribed C_μ. The prescribed C_μ is achieved by adjusting the injection cavity total pressure. Total temperature is assumed constant during this process. The injection and suction mass flow are matched by adjusting the suction cavity static pressure. The process is iterated throughout the simulation until the specified momentum coefficient is reached and the injection and suction mass flow match within the tolerance of 1%.

5.3 Mesh

The CFJ-EA mesh, shown in Fig. 5, is constructed using a cylindrical mesh topology, around the plane fuselage. The cylindrical topology is interrupted by the main wing which is enclosed in a O-mesh topology with 240 points around the airfoil, 40 points in the direction normal to the wall completed by an additional 40 points in the jet region, and 80 points in the spanwise direction. In a similar manner

the horizontal tail is also enclosed in an O-mesh with 120 points around the airfoil, 40 points in the direction normal to the wall and 60 points in the spanwise direction. The total mesh size is 10.4 millions points, splitted into 225 blocks for parallel computation. The far field boundary is located 30 fuselage length away from the plane. The first grid point is placed at $y^+ \approx 1$ except on the wing and tail tip walls where $y^+ \approx 50$ is used with the wall function boundary condition to reduce the mesh size. The baseline EA without CFJ is constructed using the same mesh topology. The main wing O-mesh has a smaller mesh size due to the absence of jets and is constructed with 160 points around the airfoil, 40 points in the direction normal to the wall and 80 points in the spanwise direction. The total mesh size is 8.2 millions points, splitted into 166 blocks for parallel computation. A similar mesh topology is used on the DLR-F6 wing/body drag prediction to benchmark our code. The coefficient of lift, drag, and moment are in good agreement with the experiment.

6 Results

The aerodynamic performance, the energy expenditure and the aircraft stability are studied for the baseline and the CFJ-EA at cruise and TOL condition.

6.1 Cruise Condition with Low C_μ

The CFJ-EA surface pressure contours with streamlines are plotted in Fig. 6 for the cruise condition, which is $AoA = 5°$ and $C_\mu = 0.04$. The stagnation region is centered on the aircraft nose. From there, the flow curves around the cabin with a small upward component, which increases the local incidence of the wing. The local lift loading is maximum in the inner section of the wing as shown by the low pressure in deeper blue color. The wing tip is affected by the downwash generated by the wing tip vortices, which reduces the tip loading, as shown by the lighter blue color. The wing suction surface streamlines in Fig. 6 indicates that the jet is well aligned with the main flow. This is very desirable to make CFJ effective and reduce the energy expenditure.

The horizontal tail role is to generate enough downforce for the aircraft to be stable during cruise but not so much as to decrease the overall aircraft performance. The present CFJ-EA design horizontal tail AoA is 0, but its incidence is slightly negative due to the wing and fuselage downwash as visualized on Fig. 6 by the slightly downward streamlines direction. Hence the horizontal tail generates a slight downforce during cruise.

The local lift loading can be further seen on the pressure coefficient (Cp) and isentropic Mach number plots shown in Figs. 7 and 8. The spikes at 3% and 80% chord correspond to the injection and suction location respectively, where the surface of the airfoil is discontinuous. Both plots show that the lift loading is fairly uniform in the inner 85% span, while the outer 15% span loading is decreased due to tip vortex. The CFJ airfoil has a high suction peak near the LE, which contributes to the lift increase and the pressure drag decrease. The lowest Cp and isentropic Mach number achieved are -2.1 and 0.26 respectively.

The CFJ-EA Mach contours with streamlines are plotted for the cruise condition at different spanwise locations in Fig. 9. Note that the color map range for the three fuselage sections is a little different from the three wing sections to best highlight their flow feature. As can be seen in Fig. 9, the fuselage generates some lift due to the convex shape of the fuselage upper surface, which also makes the air flow upward. This upward flow increases the local incidence of the wing in the vicinity of the fuselage. As mentioned earlier, the tail generates a small negative lift due to the downwash. The T-tail configuration reduces the interaction of the horizontal tail with the aircraft wake and downwash. It also suppresses the tip vortex of the vertical tail and increases the vertical tail control effectiveness. The CFJ wing

wake is energized by the jet and remain very small. The 99% span flow field shows the influence of the wing tip vortex, which reduces the tip lift loading.

The lift, drag and moment coefficients for the EA at cruise Mach number are shown in Fig. 10. As a comparison, the baseline airplane, which uses the original NACA 6415 airfoil with no CFJ for the wing, is also simulated. At constant AoA, the CFJ-EA C_L is significantly higher than the baseline EA. Higher C_μ yields a higher lift coefficient. In addition, the use of CFJ delays the stall AoA from 10° for the baseline EA to 20° for the CFJ-EA at $C_\mu = 0.08$. The maximum C_L is increased from 1.5 for the baseline EA to 2.6 for the CFJ-EA at $C_\mu = 0.08$. For all C_μ, the drag of the CFJ-EA is significantly lower than the baseline EA until the stall AoA is reached.

The CFJ-EA is trimmed in cruise condition, which is at M=0.15, $AoA = 5°$ and $C_\mu = 0.04$. If we calculate the aircraft Static Stability Margin (SSM) with the following formulation :

$$SSM = -\frac{dC_m/d\alpha}{dC_l/d\alpha} = -\frac{dC_m}{dC_l} \tag{20}$$

both the baseline and CFJ-EA are statically stable in pitch with a cruise SSM of 0.36 and 0.29 respectively. The use of CFJ decreased the cruise SSM by about 0.07, but the remaining SSM is more than enough to maintain the aircraft stability.

The aerodynamic efficiency and energy consumption for the EA at cruise Mach number are shown in Fig. 11. The power coefficient is calculated assuming an efficiency of 85% for the pump based on equations 8 and 9. The minimum Pc is 0.012 for $C_\mu = 0.04$ at $AoA = 10°$. When the C_μ is increased, the power consumption is dramatically increased. The minimum power consumption AoA is increased with the C_μ. The baseline configuration reaches a peak aerodynamic L/D of 22.5 during cruise condition. The CFJ-EA reaches a peak L/D of 36.3 at $C_\mu = 0.04$ and up to 64.6 at $C_\mu = 0.08$. The peak $(L/D)c$ for the CFJ-EA at $C_\mu = 0.04$ is higher than the baseline aircraft L/D peak, suggesting that the overall energy efficiency of the aircraft is improved with the use of CFJ. This is also the reason that the $C\mu = 0.04$ is chosen for cruise. When the C_μ is increased, the aerodynamic L/D continue to increase. However the $(L/D)c$ is decreased because of the increased power consumption. Similarly to the Pc behavior, the peak $(L/D)c$ of the CFJ-EA is shifted toward higher AoA when the C_μ is increased.

The CFJ-EA cruises at a very high C_L of 1.3, which produces a wing loading of $182.3 kg/m^2$, about 3 times higher than that of a conventional general aviation airplane. The excellent cruise $(L/D)_c$ of 24 combined with the high cruise wing loading give the CFJ-EA an exceptionally compact size airplane, with high payload and long range.

6.2 Takeoff/Landing Condition with High C_μ

In order to evaluate the TOL performance, we simulate the behavior of the CFJ-EA at high AoA and high C_μ. The calculations are performed at M=0.1 to simulate the typical TOL velocity of a general aviation airplane.

The CFJ-EA surface isentropic Mach contours with streamlines are plotted in Fig. 12 for the TOL condition, which is $AoA = 25°$ and $C_\mu = 0.24$. The fuselage lift is enhanced by the lower stagnation region location, just under the aircraft nose, and the relatively large flow acceleration on the top surface of the cabin. The wing is significantly loaded, as indicated by the very high isentropic Mach number at the wing LE and the stagnation point located at a more downstream position on the pressure surface. The LE flow acceleration is much smaller in the wing tip region. Even though the horizontal tail AoA is 25°, the flow remains fully attached. This is because its incidence is much lower due to the fuselage and wing downwash.

The lift, drag and moment coefficients for the CFJ-EA in TOL condition are shown Fig. 13. A higher C_μ yield a higher lift coefficient. However, due to the strong lift-induced drag, there is a significant

drag penalty for the higher C_μ cases. The maximum C_L achieved is 4.8 at $C_\mu = 0.28$. However, to lower the power consumption and conserve a comfortable stall margin of 10°, the TOL is performed at $AoA = 25°$ with a C_μ of 0.24. In this conditions, the C_{LTO} is 3.9. With C_{Lmax}=4.8, the stall velocity is 24.55m/s(55mile/h). A reasonable TOL velocity would hence be taken as 1.2 times this value with an approximate Mach number of 0.085. We use Mach number of 0.01 as the takeoff Mach number to be conservative. The flow is also insensitive to the Mach number in this incompressible range. The case is simulated without the horizontal tail flap deflected. It is hence not trimmed at $AoA = 25°$. However, the pitching moment is small and and would be very controllable by deflecting the flap.

The aerodynamic efficiency and energy consumption for the CFJ-EA at TOL Mach number are shown in Fig. 14. As expected, the power coefficient at $C_\mu = 0.24$ is much higher than at $C_\mu = 0.04$. However, since the power consumption is proportional to V^3 (see Eq. 9), the actual power consumption increase is only about 3 times higher than at cruise due to the lower TOL speed. For a typical TOL at $AoA = 25°$ and $C_\mu = 0.24$, the aerodynamic L/D is 16.5. Such a high L/D at takeoff is made possible by the strong jet that reduces the pressure drag. In the range of AoA studied, the L/D is similar for all the different C_μ.

CFJ at high C_μ outperforms the conventional lift enhancement devices such as slats and flaps with a very high maximum lift while keeping the drag and moment low [25, 26, 27, 28]. This is because the use of CFJ generates lift and thrust at the same time, which makes it more efficient than conventional high lift systems. Thus, unlike conventional high lift systems that are used exclusively during takeoff and landing, the CFJ is used for all the flight envelope, with a high C_μ for demanding conditions like TOL or high G maneuvers, and a low C_μ during cruise.

6.3 Mission Analysis

The cruise condition is taken as M=0.15, $AoA = 5°$ and $C_\mu = 0.04$ which correspond to the aircraft near maximum $(L/D)c$. The TOL condition is taken as M=0.1, $AoA = 25°$ and $C_\mu = 0.24$ which provides a C_L value of 3.9 while still conserving a sufficient stall margin AoA of 10°. The CFJ-EA performance is compared with a reciprocating engine powered airplane and three electric airplanes in Table 1. The Cessna 172 is chosen for comparison to represent the current mainstream general aviation reciprocating engine airplane. The electric airplanes selected for comparison are the Antares 20, a motor-glider and the two state-of-the-art E-Genius, and Taurus G4. The mission analysis is performed for a payload of 364 kg for passengers and luggage. The structure factor of the CFJ-EA is taken as 45%, which means that the empty weight of the aircraft is 45% of the gross takeoff weight. The structure factor is 6% higher than that of the Taurus G4 [29] to be conservative. It is reasonable to believe that a low structure factor is achievable with modern construction materials. The batteries account for the rest of the weight of the aircraft. The batteries specific energy density of 250 Wh/kg is used in the mission analysis. It is the level of current Li-ion battery technology. The range of the EA is also calculated with a battery specific energy density of 1750 Wh/kg, which is used as the projection for the next 20 years [10]. The overall propulsion efficiency of the CFJ-EA is set at 73% to account for the efficiency of the propeller, controller, electric motor and gearbox. In addition, a pumping efficiency of 85% is used. Finally, 20% of the energy storage is reserved for the start-up, takeoff, acceleration to cruise velocity and altitude and landing. The mission analysis is performed for a takeoff at sea level, climb to cruise altitude of 5000 ft, cruise at M=0.15, descent to see level and landing. More information about the mission analysis calculations can be found in [13].

As seen in Table 1, the CFJ-EA cruises at a $(L/D)c$ of about 24, which is slightly lower than the aerodynamic L/D the other EAs. Compared with the Taurus G4 that also carries 4 passengers, the wing area of the present CFJ-EA is 50% smaller and the lift coefficient is 2.6 times greater. As a result, its wing loading reach an outstanding $182.3 kg/m^2$. This allows the CFJ-EA to carry the more battery,

even though its wing size is smaller. The large amount of battery and excellent cruise $(L/D)c$ allow the CFJ-EA to achieve an outstanding range of 292nm. This range compares very favorably with the 250nm range of the Taurus G4, or the 216nm of the E-Genius. In addition, TOL performance is very good due to the very high C_{LTO} of 3.9. If, in the near future, the projected power and energy density of the battery increase 7 fold, as anticipated in [10] the range of the present CFJ-EA could reach 2000+nm. This is a very significant range, even compared with today's general aviation standards like the Cessna 172 and its 700nm range.

7 Conclusion

The conceptual design of the electric airplane utilizing Co-Flow Jet (CFJ) flow control presented in this paper achieves a very high wing loading and a compact size with an excellent aerodynamic efficiency. The CFJ-EA mission is to carry 4 passengers with the range close to 300nm with a cruise Mach number of 0.15 and a takeoff velocity of 24.6m/s. The CFJ-EA cruises at an outstanding C_L of 1.3 with C_μ of 0.04, which provides the aircraft with a remarkable wing loading of $182.3kg/m^2$, about three times higher than the conventional general aviation aircraft. The cruise L/D is 36 and the aerodynamic efficiency (L/D)c, which takes into account the power coefficient of the pump, is 24. In addition, the design is stable in pitch with a static stability margin of 29%. Unlike conventional high lift systems, which are used exclusively during takeoff and landing, the CFJ wing is used for all the flight envelope with a low pumping power at cruise and high pumping power at takeoff and landing. The CFJ-EA achieves a remarkable maximum C_L of 4.8, which shortens the takeoff/landing distances. Due to the increased wing loading and reduced size, the parameter PMS= Passenger*Miles/S, is close to that of a conventional reciprocating engine airplane and is about 2.3-3.8 times higher than that of the state of the art EA. This design is the first trail without any design optimization. It is believed that the aircraft performance can be further improved with design optimization. The CFJ-EA concept may open the door to a new class of general aviation EA designs to significantly increase range with a compact size. The same CFJ flow control technology can also be used for airplanes with conventional propulsion systems and the high cruise altitude airplanes to reduce the wing size.

References

[1] G.-C. Zha and D. C. Paxton, "A Novel Flow Control Method for Airfoil Performance Enhancement Using Co-Flow Jet." *Applications of Circulation Control Technologies*, Chapter 10, p. 293-314, Vol. 214, Progress in Astronautics and Aeronautics, AIAA Book Series, Editors: Joslin, R. D. and Jones, G.S., 2006.

[2] G.-C. Zha, W. Gao, and C. Paxton, "Jet Effects on Co-Flow Jet Airfoil Performance," *AIAA Journal, No. 6,*, vol. 45, pp. 1222–1231, 2007.

[3] G.-C. Zha, C. Paxton, A. Conley, A. Wells, and B. Carroll, "Effect of Injection Slot Size on High Performance Co-Flow Jet Airfoil," *AIAA Journal of Aircraft*, vol. 43, 2006.

[4] G.-C. Zha, B. Carroll, C. Paxton, A. Conley, and A. Wells, "High Performance Airfoil with Co-Flow Jet Flow Control," *AIAA Journal*, vol. 45, 2007.

[5] Wang, B.-Y. and Haddoukessouni, B. and Levy, J. and Zha, G.-C., "Numerical Investigations of Injection Slot Size Effect on the Performance of Co-Flow Jet Airfoil," *Journal of Aircraft*, vol. 45, No. 6, pp. 2084–2091, 2008,.

[6] B. P. E. Dano, D. Kirk, and G.-C. Zha, "Experimental Investigation of Jet Mixing Mechanism of Co- Flow Jet Airfoil." AIAA-2010-4421, 5th AIAA Flow Control Conference, Chicago, IL, 28 Jun - 1 Jul 2010.

[7] B. P. E. Dano, G.-C. Zha, and M. Castillo, "Experimental Study of Co-Flow Jet Airfoil Performance Enhancement Using Micro Discreet Jets." AIAA Paper 2011-0941, 49th AIAA Aerospace Sciences Meeting, Orlando, FL, 4-7 January 2011.

[8] A. Lefebvre, B. Dano, M. D. Fronzo, W. B. Bartow, and G-C. Zha, "Performance of a Co-Flow Jet Airfoil with Variation of Mach Number," *AIAA paper 2013-490*, Jan 2013.

[9] A. Lefebvre, G-C. Zha, "Numerical Simulation of Pitching Airfoil Performance Enhancement Using Co-Flow Jet Flow Control," *AIAA paper 2013-2517*, June 2013.

[10] M. Hepperle, "Electric Flight - Potential and Limitations." NATO-OTAN MP-AVT-209-09, 2012.

[11] J. Aguirre and G.-C. Zha, "Design and Study of "Engineless" Airplane Using Co-Flow Jet Airfoil." AIAA Paper 2007-4441, June 2007.

[12] S. Aspe, J.J. Dussling, N. R. Heinz, D. J. Martinez, Adviser: Gecheng Zha, " The 2058 Aircraft: Quiet Ultra-Efficient Integrated Aircraft (QUEIA)." The second place, 2008 University Student Competition, NASA, http://aero.larc.nasa.gov/competitions_univ.htm, May 2008.

[13] A. Lefebvre, "Investigation of Co-Flow Jet Flow Control and its Applications." Ph.D. Thesis, University of Miami, June 2015.

[14] P. Spalart and S. Allmaras, "A One-equation Turbulence Model for Aerodynamic Flows." AIAA-92-0439, 1992.

[15] Y.-Q. Shen and G.-C. Zha, "Large Eddy Simulation Using a New Set of Sixth Order Schemes for Compressible Viscous Terms ," *Journal of Computational Physics*, vol. 229, pp. 8296–8312, 2010.

[16] G.-C. Zha, Y. Shen, and B. Wang, "An improved low diffusion E-CUSP upwind scheme ," *Journal of Computer & Fluids*, vol. 48, pp. 214–220, 2011.

[17] Y.-Q. Shen and G.-Z. Zha , "Generalized finite compact difference scheme for shock/complex flowfield interaction," *Journal of Computational Physics*, vol. doi:10.1016/j.jcp.2011.01.039, 2011.

[18] Shen, Y.-Q. and Zha, G.-C. and Wang, B.-Y., " Improvement of Stability and Accuracy of Implicit WENO Scheme," *AIAA Journal*, vol. 47, No. 2, pp. 331–344, 2009.

[19] Shen, Y.-Q. and Zha, G.-C. and Chen, X.-Y., " High Order Conservative Differencing for Viscous Terms and the Application to Vortex-Induced Vibration Flows," *Journal of Computational Physics*, vol. 228(2), pp. 8283–8300, 2009.

[20] Shen, Y.-Q. and Zha, G.-C. , " Improvement of the WENO Scheme Smoothness Estimator," *International Journal for Numerical Methods in Fluids*, vol. DOI:10.1002/fld.2186, 2009.

[21] G.-C. Zha and E. Bilgen, "Numerical Study of Three-Dimensional Transonic Flows Using Unfactored Upwind-Relaxation Sweeping Algorithm," *Journal of Computational Physics*, vol. 125, pp. 425–433, 1996.

[22] B.-Y. Wang and G.-C. Zha, "A General Sub-Domain Boundary Mapping Procedure For Structured Grid CFD Parallel Computation," *AIAA Journal of Aerospace Computing, Information, and Communication*, vol. 5, No.11, pp. 2084–2091, 2008.

[23] Wang, B. Y and Zha, G.-C. , "Detached-Eddy Simulation of a Co-Flow Jet Airfoil at High Angle of Attack." AIAA Paper 2009-4015, AIAA Journal of Aircraft, Vol. 48, No. 5, 2011, 2011.

[24] Y.-Q. Shen, G.-C. Zha, and B.-Y. Wang, "Improvement of Stability and Accuracy of Implicit WENO Scheme ," *AIAA Journal*, vol. 47, pp. 331–344, 2009.

[25] A. Lefebvre, G-C. Zha, "Cow-Flow Jet Airfoil Trade Study Part I : Energy Consumption and Aerodynamic Performance," *AIAA paper 2014-2682*, June 2014.

[26] A. Lefebvre, G-C. Zha, "Cow-Flow Jet Airfoil Trade Study Part II : Moment and Drag," *AIAA paper 2014-2683*, June 2014.

[27] T. A. Harris and R. S. Swanson, "Wind-tunnel tests of an NACA 23021 airfoil equipped with a slotted extensible and plain extensible flap ." Technical Note No. 782, NACA, November 1940.

[28] T. A. Harris and I. G. Recant, "Wind-tunnel investigation of NACA 23012, 23021 and 23030 airfols equipped with 40 percent chord double slotted flaps." Report No. 723, NACA, 1941.

[29] Jack W. Langelaan, Anjan Chakrabarty, Aijun Deng and Kirk Miles, "Green Flight Challenge: Aircraft Design and Flight Planning for Extreme Fuel Efficiency," *Journal of aircraft*, vol. Vol. 50, No. 3, pp. 832–846, May-June 2013.

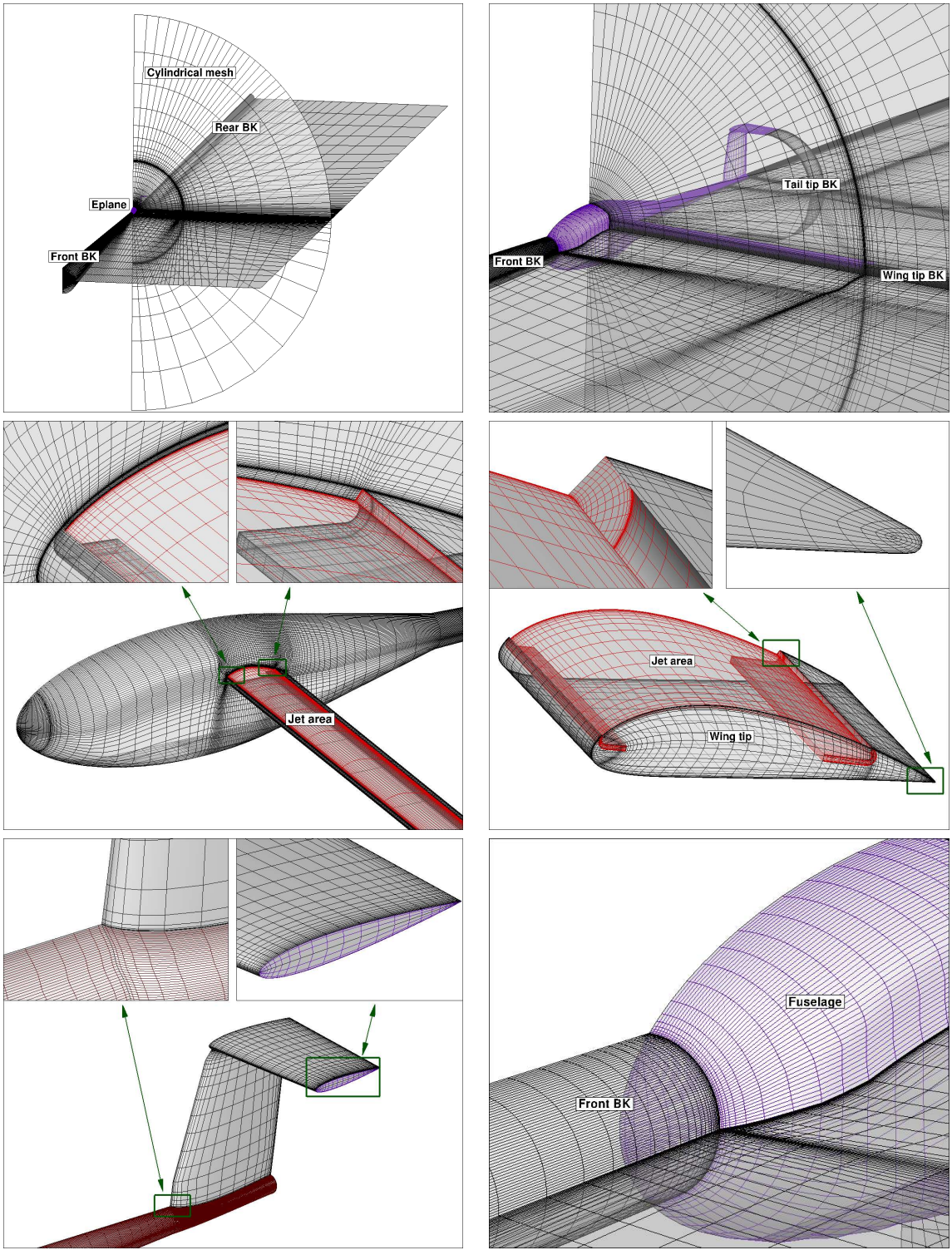

Figure 5: Mesh overview for the CFJ-EA. Only one mesh point out of two is displayed for clarity.

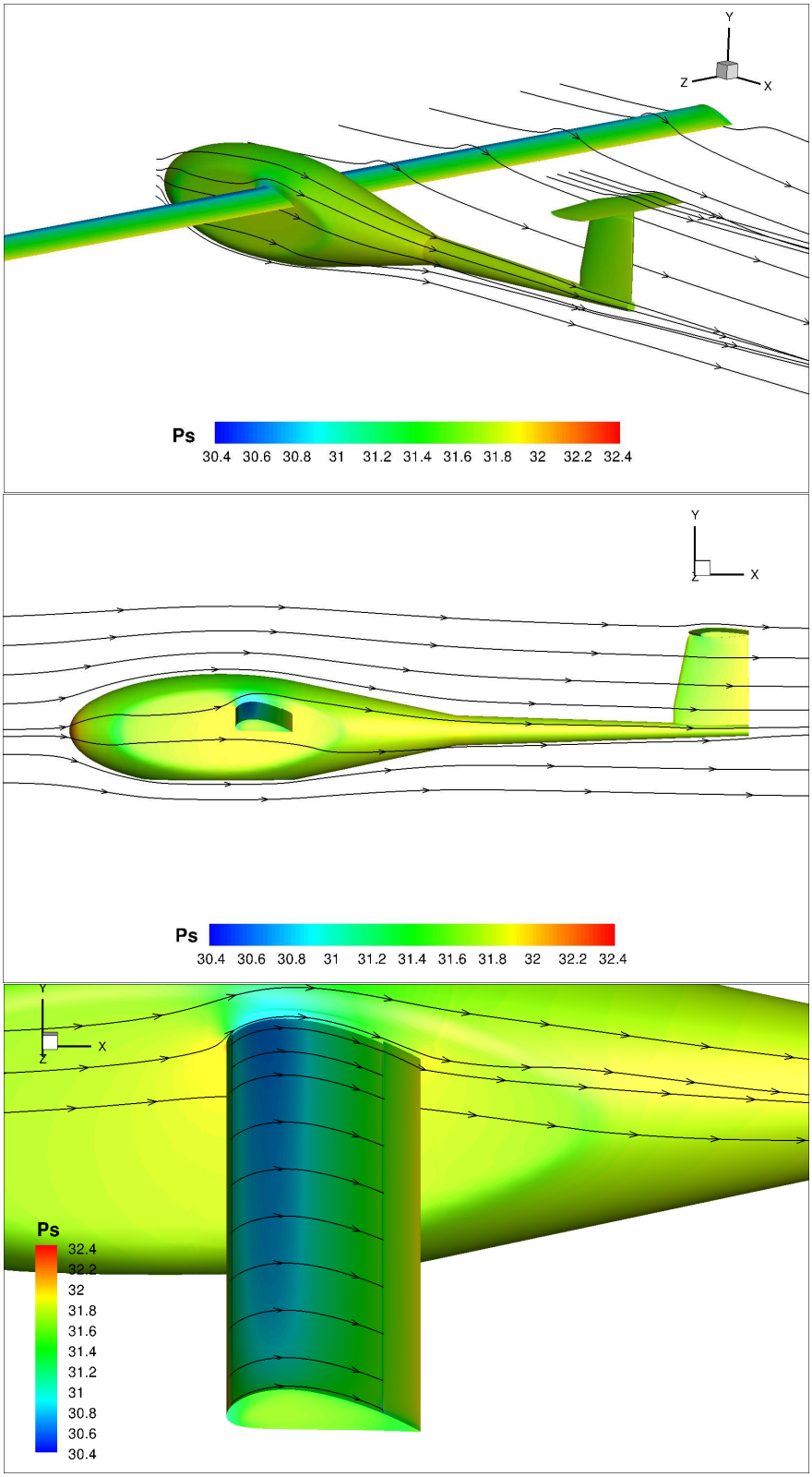

Figure 6: Surface pressure contours, cruise conditions, $C_\mu = 0.04$ and $AoA = 5°$.

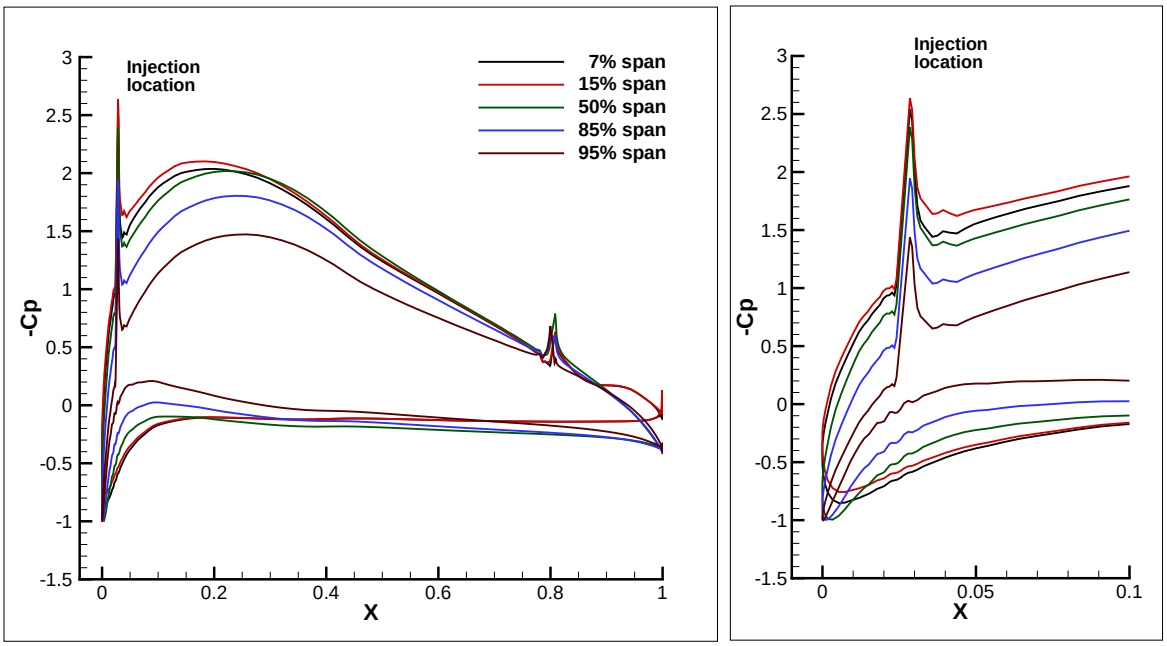

Figure 7: Cp at different spanwise locations, cruise conditions, $C_\mu = 0.04$ and $AoA = 5°$. The 7% spanwise location corresponds to the wing root.

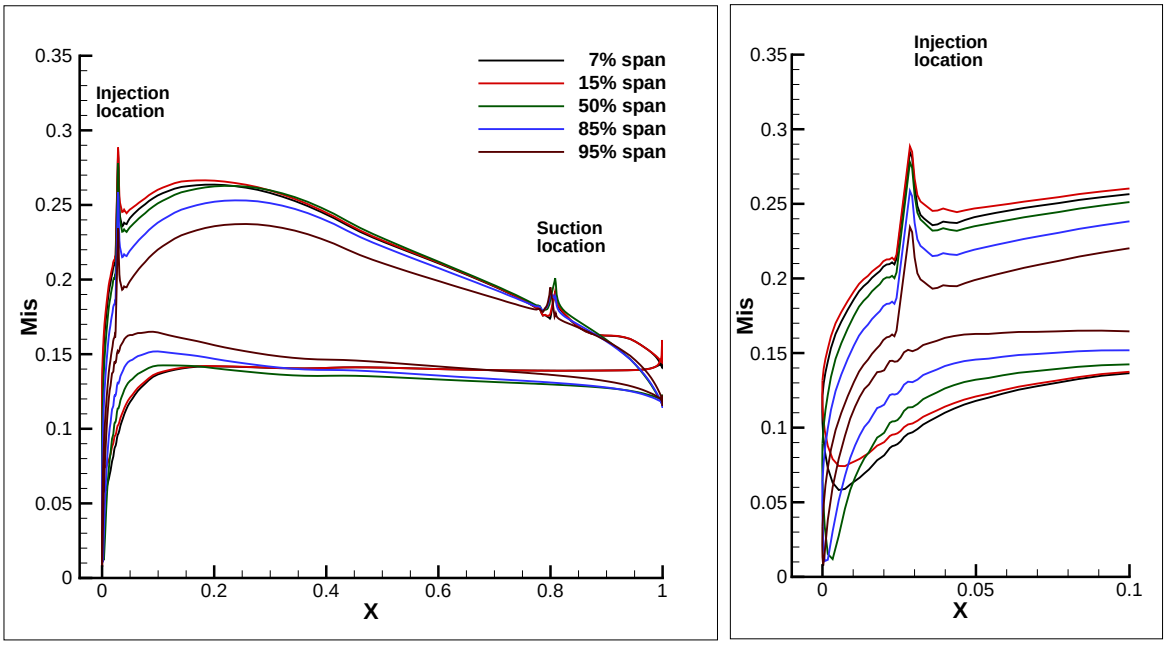

Figure 8: Isentropic Mach number at different spanwise locations, cruise conditions, $C_\mu = 0.04$ and $AoA = 5°$. The 7% spanwise location corresponds to the wing root.

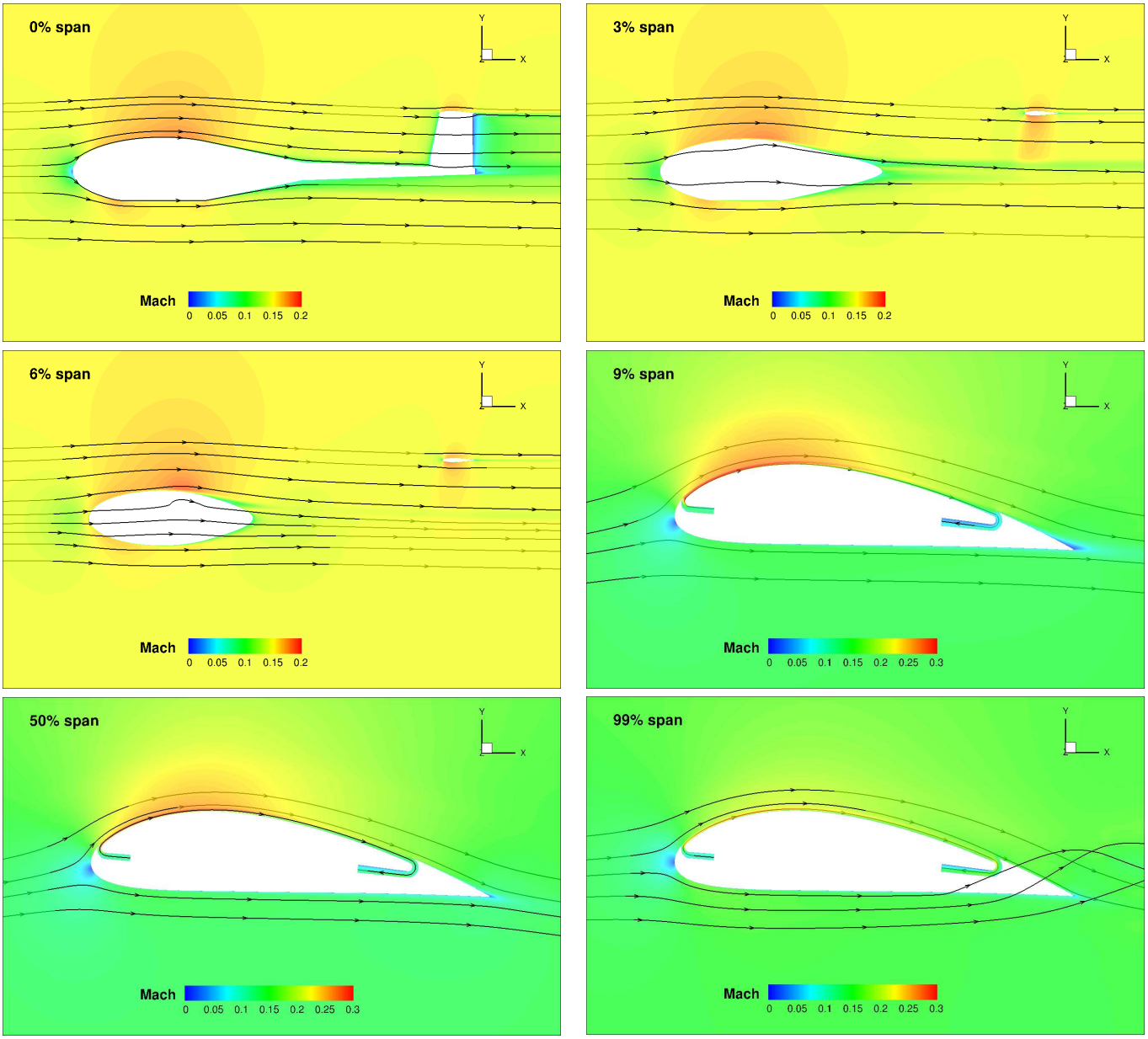

Figure 9: Eplane Mach contours at various spanwise locations, cruise conditions, $C_\mu = 0.04$ and $AoA = 5°$.

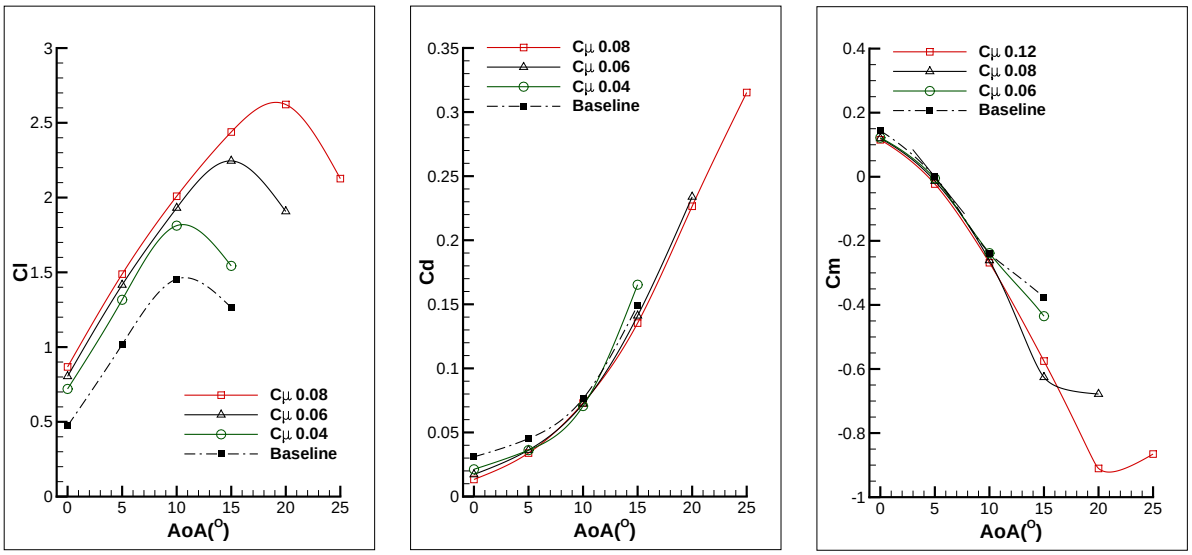

Figure 10: Forces and moment versus AoA, simulations performed at M=0.15, $0.04 \leq C_\mu \leq 0.08$.

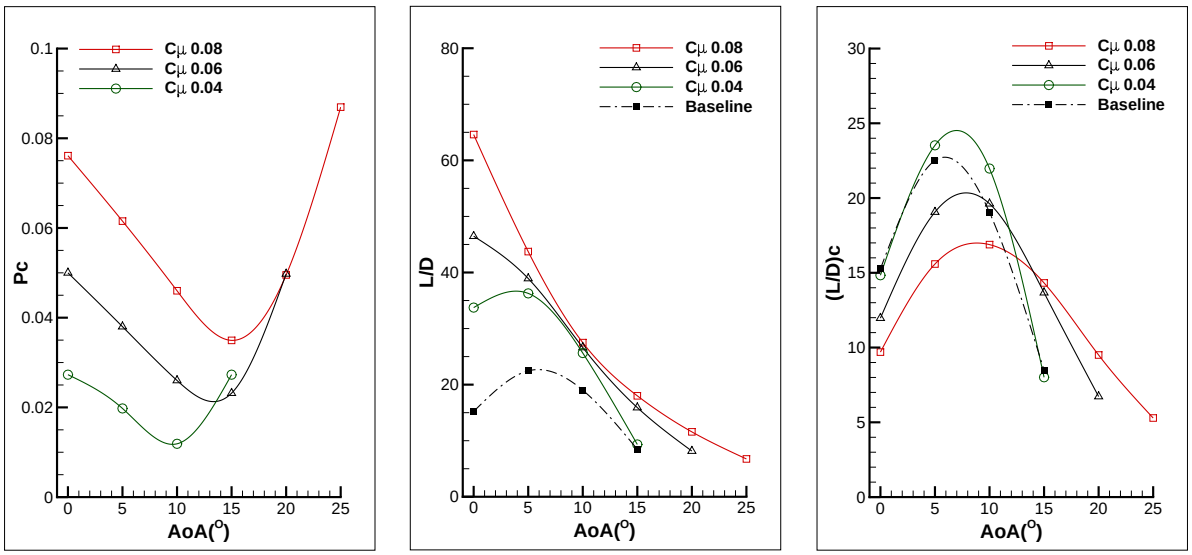

Figure 11: Energy expenditure and aerodynamic efficiency versus AoA, simulations performed at M=0.15, $0.04 \leq C_\mu \leq 0.08$.

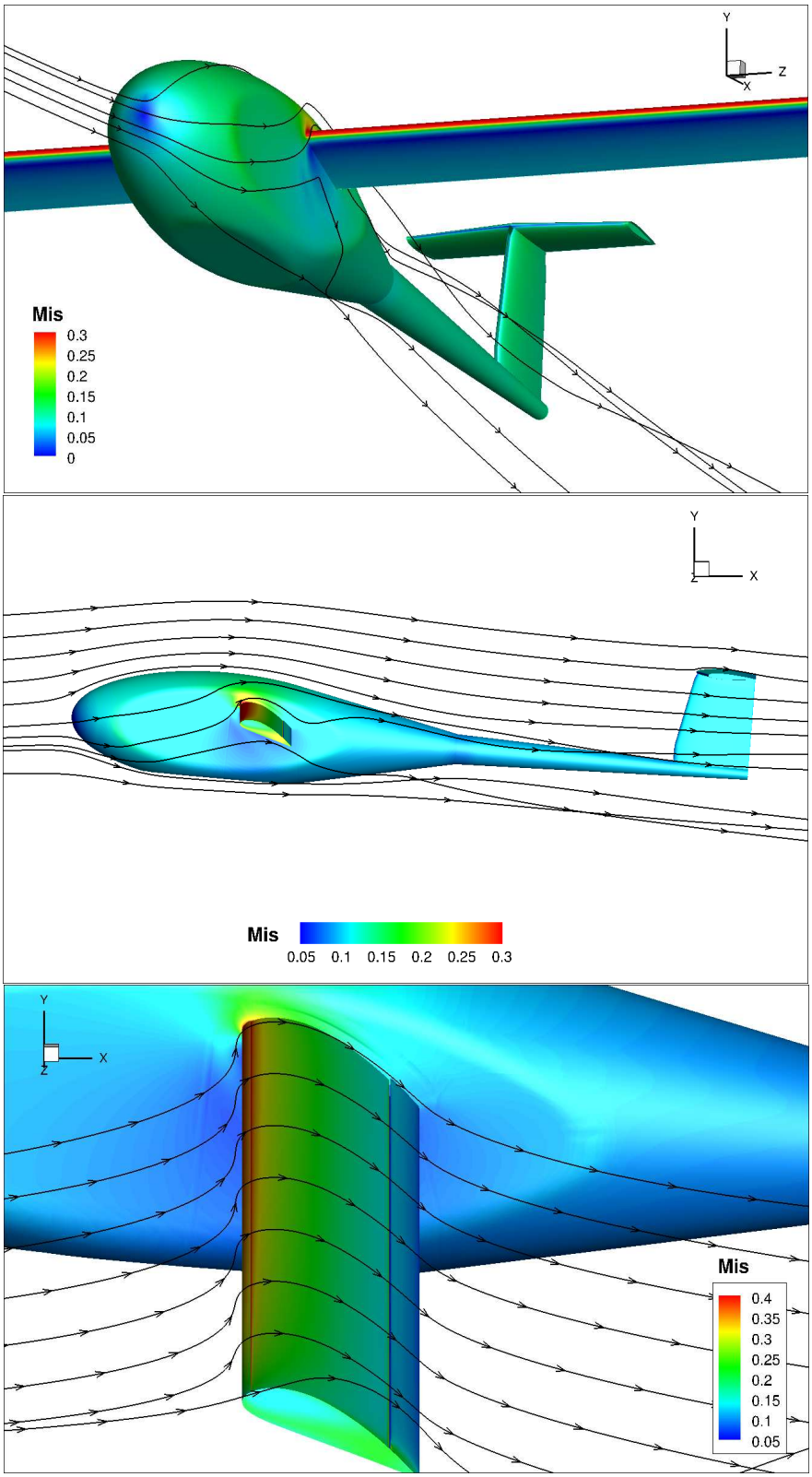

Figure 12: Eplane isentropic Mach contours, takeoff/landing condition, maneuvering, simulations performed at $AoA = 15°$, M=0.10 and $C_\mu = 0.24$.

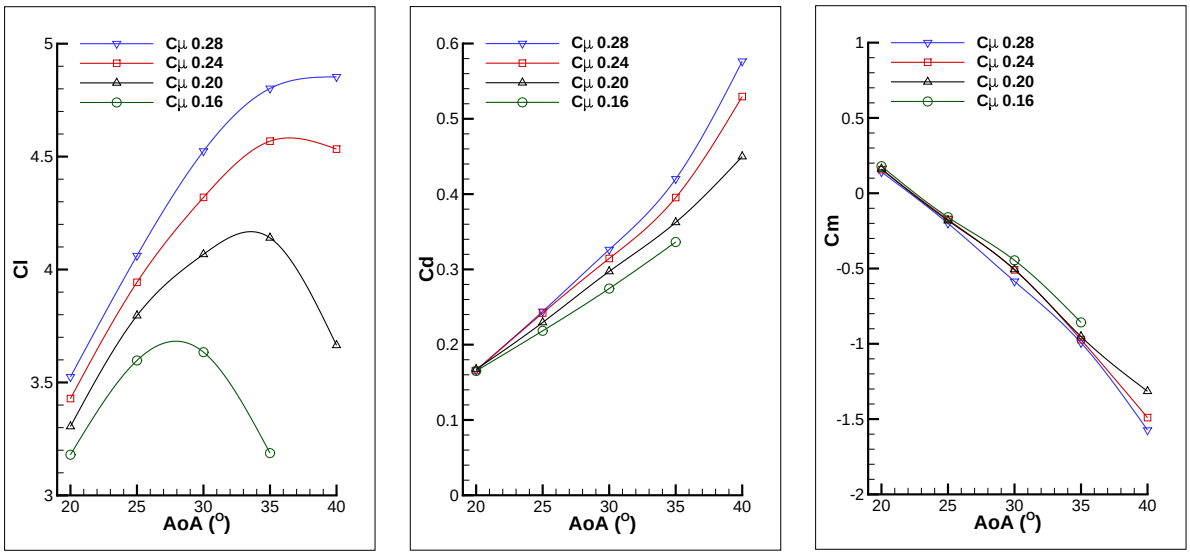

Figure 13: Energy expenditure and aerodynamic efficiency versus AoA, simulations performed at M=0.10, $0.16 \leq C_\mu \leq 0.28$

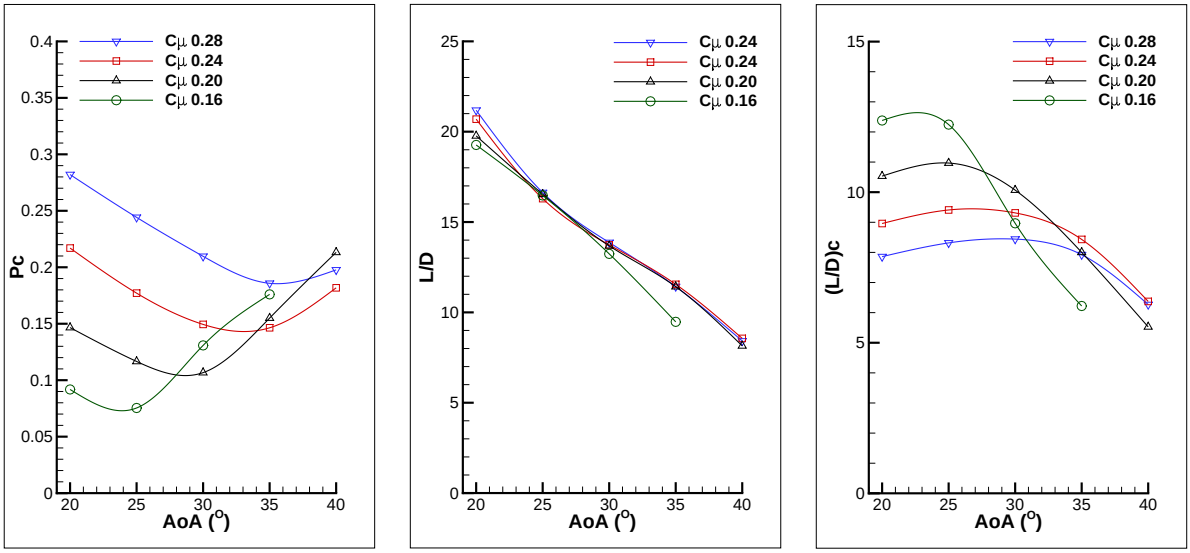

Figure 14: Energy expenditure and aerodynamic efficiency versus AoA, simulations performed at M=0.10, $0.16 \leq C_\mu \leq 0.28$

Aircraft	Cesna 172	Antares 20E	E-Genius	Taurus G4	CFJ Eplane
Geometry					
Wing span (m)	11.00	20.00	16.90	21.36	14.90
Wing area (m2)	16.20	12.60	14.56	20.30	10.44
AR	7.3	31.7	19.6	22.5	21.3
Length (m)	8.28	7.40	8.10	7.40	9.12
Cruise data					
Nb of passengers	4	1	2	4	4
CL	0.32	0.38	0.57	0.50	1.31
CD	0.046	0.013	0.020	0.018	0.036
Pc	N/A	N/A	N/A	N/A	0.014
L/D	7	30	26	28	36
L/Dc	7	30	26	28	25
Velocity (m/s)	63	51	45	51	51
Weight					
Max TO weight (kg)	1,111	660	950	1,496	1,896
Structure ratio	0.69	0.70	0.47	0.39	0.45
Structure weight (kg)	767.0	460.0	760.0	632.0	853.0
Passenger + payload (kg)	250.0	140.0	182.0	364.0	364.0
Battery weight (kg)	N/A	60.0	310.0	500.0	678.5
Aircraft	**Cesna 172**	**Antares 20E**	**E-Genius**	**Taurus G4**	**CFJ Eplane**
Propulsion / Battery					
Propulsion eff (%)	39	73	73	73	73
Pump efficiency (%)	N/A	N/A	N/A	N/A	85
Battery specific E (Wh/Kg)	N/A	136	180	180	250
Energy available (kWh)	2,212.0	8.2	56.0	90.0	169.6
Propeller power cruise (kW)	251.6	15.2	17.6	32.0	35.7
CFJ power cruise (kW)	N/A	N/A	N/A	N/A	10.34
Total power drawn cruise (kW)	251.6	15.2	17.6	32.0	46.0
Performance					
Range (nm)	700	43	216	250	292
nm*passenger/S	172.8	3.4	29.7	49.3	112.4
mpg*passengers	57.5	236.8	350.7	505.1	313.2
Crusie time (h)	5.7	0.4	2.5	2.5	2.9
Projected range in 20 year (n	700	298	1512	1750	2046
Wing loading (kg/m2)	68.6	52.9	61.8	69.6	182.3
TO CL	2.0	1.6	1.8	1.8	3.5
TO distance (ft)	1700	1900	1700+	2000	2000

Table 1: Comparisons of the present CFJ-EA with Cessna 172 reciprocating engine airplane and three state of the art electric airplanes. Some of the data are estimations only.